

Momentum vector correlations in three-particle fragmentation of triatomic hydrogen

H. Höffler, P. C. Fechner, M. Gisi, F. Baumgartner, U. Galster, and H. Helm

Department of Molecular and Optical Physics, Albert-Ludwigs-Universität, Hermann-Herder Straße 3, D-79104 Freiburg, Germany

(Received 27 January 2011; published 29 April 2011)

The correlation pattern in the center of mass motion of the three fragments from dissociation of well-defined Rydberg states of H_3 and D_3 is studied. Dissociation of the molecules is induced by an external electric field. Through a comparison with results obtained in radiative cascading we can show that the correlation pattern is that of the short-lived $2s\ ^2A_1'$ electronic state, of which a tiny amplitude is admixed by the external electric field. A comparison of our results with the predictions by M. Lehner and M. Jungen [*J. Phys. B* **42**, 065101 (2009)] and U. Galster [*Phys. Rev. A* **81**, 032517 (2010)] for predissociation of the $2s\ ^2A_1'$ state is made. We show that the experimental vector correlation maps are direct images of the spatial symmetry of the product of the vibrational wave function and spatial dependence of the nonadiabatic coupling operator.

DOI: [10.1103/PhysRevA.83.042519](https://doi.org/10.1103/PhysRevA.83.042519)

PACS number(s): 31.50.Gh, 33.80.Gj

I. INTRODUCTION

A frequent origin for dynamic change of molecules is nonadiabaticity in the form of coupling between bound and continuum states. Triatomic molecules show a distinct signature of such coupling in the decay into three fragment atoms. This signature is unique if the three atoms are in their electronic ground state. The gist is that in predissociation of the molecule all molecular information is projected into the correlation between the three atomic momentum vectors. Here we study the decay of isolated H_3 and D_3 molecules into three ground-state hydrogen atoms and monitor the vector correlation of the three atomic fragment momenta. We show that the maps of vector correlation are a direct image of the product of the molecular vibrational wave function and the spatial part of the nonadiabatic coupling operator.

To view this subject from another angle we consider the analogy of such an experiment to Young's double slit, where an initial state and an aperture function lead to an experimental diffraction pattern. In the double-slit experiment the initial state is the k -vector of incoming particles while the aperture function describes size and location of the slits. From the experimental pattern and knowledge of the initial state a reconstruction of the aperture function can be attempted.

The analogy to the experiment presented here is as follows: Our initial state is the Rydberg molecule prepared in a set of quantum numbers. These dictate the electronic and nuclear motion in the phase space of the bound molecule. The aperture function appears as the map of nonadiabatic pathways which lead from the bound state into the continuum of three separated atoms. For three ground-state atoms this final-state phase space has only five dimensions, two of the relative motion of the three atoms in the plane containing the center of mass of the dissociated molecule and three Euler angles describing the orientation of this plane in the laboratory. This space is filled with the diffraction pattern which emerges from the time-dependent product of the initial molecular state and the nonadiabaticity, the aperture function. From this viewpoint a clear challenge emerges to the experimenter. Defining the initial state with the precision allowed by quantum mechanics and recording the final-state diffraction pattern in a precise fashion may eventually enable the experimental reconstruction

of the aperture function, thus providing experimental access to nonadiabatic couplings.

In this context it is most exciting that predictions for momentum vector correlation maps of the three-particle decay of H_3 and D_3 have recently become available from theory [1,2]. Theory specifically considered the short-lived $2s\ A_1'$ Rydberg state, neglecting rotation, as the electronic initial state, and has combined the quantum description of the bound Rydberg state and its nonadiabatic transition operator with classical trajectories on the two Jahn-Teller-split ground-state surfaces. To check the validity of these predictions we have begun to explore Dalitz maps of the short-lived $2s\ A_1'$ state. This electronic state is not easily amenable to direct photoexcitation and has hence not been a topic of scrutiny in the past. We have found ways to prepare H_3 molecules in selected vibrational levels of the $2s$ state, based on Stark field mixing and on populating $2s$ levels in cascading dipole transitions. Here we report these experiments and compare the momentum vector correlation maps obtained with the maps predicted by theory. This comparison leads us to a first direct interpretation of the dominant features in the correlation maps.

II. EXPERIMENT AND METHODS

Multidimensional imaging and coincidence techniques allow us to tackle the three-body dissociation problem experimentally, providing information about correlation in fragment momentum vectors [3–6]. The basic experimental setup used in Freiburg for neutral triatomic hydrogen is shown Fig. 1. A 3 keV beam of mass-selected ions passes through a charge transfer cell filled with cesium vapor. By accepting an electron from the cesium atoms, the mass-selected ions are converted into neutral molecules, primarily into excited Rydberg states. About 30 cm downstream from charge transfer, the fast neutral beam passes through a 1 mm diameter aperture. Only molecules in states which are immune to immediate dissociation survive the time of flight of $\sim 1\ \mu\text{s}$ and pass the aperture. As the ground state of triatomic hydrogen is dissociative, the neutral molecular beam beyond the aperture contains only long-lived molecules. These are molecules in the metastable $2p\ ^2A_2''$ state in a variety of vibrational levels, their rotational state being $N = 0$ (as only these levels are metastable [9]), and long-lived molecules in Rydberg states

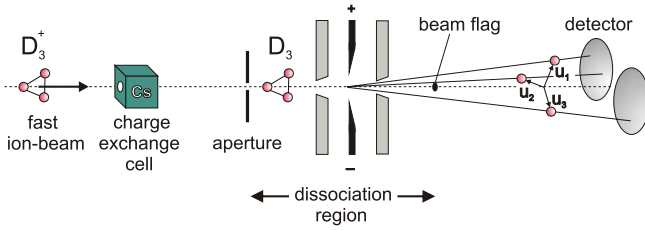


FIG. 1. (Color online) Experimental setup for D_3 . The geometrical dimensions of the Stark-field section are given in [7]. For the measurements with H_3 a slightly different Stark-field section with bigger electrodes has been used; see Fig. 2 of [8].

with high principal quantum numbers, $n \geq 6$ [7]. Here we concentrate on molecules in the metastable $2p^2A_2''$ state. As will be shown below, these serve to study the nonadiabatic coupling of the $2s^2A_1'$ state with the three-body continuum.

Beyond the aperture in Fig. 1 we apply a high electric field, localized over a 3 mm long spatial region, to induce dissociation by Stark-mixing of the long-lived states with energetically close-lying short-lived $2s^2A_1'$ levels [7,8]. After dissociation the fragments fly through a 2.40 m drift length before impinging on the position- and time-sensitive detector. A beam flag is used to prevent undissociated molecules to continue toward the detector. This reduces background from unimolecular decay. From the six impact coordinates and two arrival time differences which are monitored in coincidence for each molecule undergoing three-body decay, the kinetic energy release and the momentum vector correlation are calculated. The specific states which we study here are shown in the energy diagram in Fig. 2.

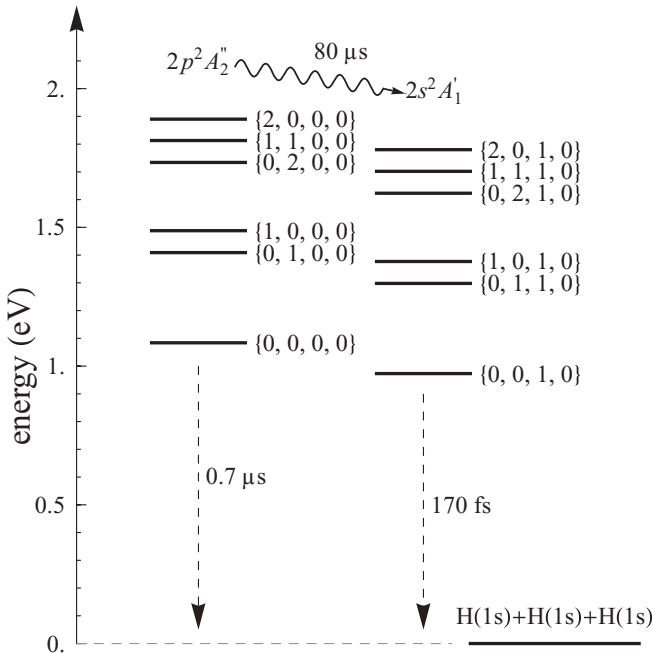


FIG. 2. Energy levels studied in this work with the example of H_3 . The state label is $\{v_1, v_2, N, K\}$ where v_1 denotes the symmetric stretch mode excitation, v_2 the degenerate bending mode, N the total angular momentum disregarding spins, and K its projection along the figure axis.

A. Stark-enhanced dissociation

Dissociation of the metastable $2p^2A_2''$ states can be induced by mixing with the nearby short-lived $2s^2A_1'$ levels. For brevity we use in the following the notation $2p$ for $2p^2A_2''$ and $2s$ for $2s^2A_1'$. The perturbed wave function in first order is

$$|2p\rangle' = |2p\rangle + \sum_i \frac{\langle i|W|2p\rangle}{E_{2p} - E_i} |i\rangle, \quad (1)$$

where $W = qz\mathcal{E}$ is the Stark operator with \mathcal{E} being the electric field strength, q the elementary charge, and z the electron spatial coordinate. The summation index i runs over all states but the $2p$ state. Neglecting all summands except the $2s$ state of the same vibrational quantum numbers yields

$$|2p\rangle' = |2p\rangle + \alpha |2s\rangle, \quad (2)$$

where

$$\alpha = \frac{\langle 2s|qz|2p\rangle}{E_{2p} - E_{2s}} \mathcal{E} \quad (3)$$

is a measure of the Stark admixture. As the fields used in our experiment are at their maximum 20 kV/cm, α stays below 0.01. Thus the energy shift due to the perturbation is negligibly small.

The small Stark admixture however rapidly increases the dissociation rate of the metastable molecules. This is due to the huge difference in lifetimes of the unperturbed states. The metastable lifetimes are $\tau_{2p} = 0.7 \mu s$ ($0.8 \mu s$) for H_3 and D_3 , respectively [10,11]. On the other hand $\tau_{2s} = 170$ fs (850 fs) for H_3 and D_3 , respectively [11]. On this basis we calculate the field-induced dissociation rate of the perturbed $2p$ state to be

$$R'_{2p}(\alpha) = \frac{1}{\tau_{2p}} + \alpha^2 \frac{1}{\tau_{2s}} = R_{2p} \left(1 + \frac{\tau_{2p}}{\tau_{2s}} \alpha^2 \right), \quad (4)$$

where R_{2p} is the dissociation rate of the unperturbed $2p$ state. Using the energy gap $E_{2p} - E_{2s} = 0.004$ a.u. [6] and the transition moment $|\langle 2s|qz|2p\rangle| = 2.689$ a.u. [12], we estimate a field-induced increase of the dissociation rate at $\mathcal{E} = 20$ kV/cm of

$$R'_{2p}/R_{2p} = 25 \quad \text{and} \quad R'_{2p}/R_{2p} = 7.4 \quad (5)$$

for H_3 and D_3 , respectively. Hence even the very small coefficient $\alpha_{20\text{kV/cm}} = 0.0026$ leads to a significant increase in the dissociation rate of metastable molecules.

This feature is born out in the experimental kinetic energy release spectra for the three-particle decay given in Fig. 3 for D_3 . A similar spectrum is observed for H_3 . In the absence of the Stark field only two prominent peaks appear. Their energetic location uniquely identifies these as originating from three-particle decay of the vibrationless $2s^2A_1'(v_1=0, v_2=0)$ state and out of the vibrationally excited $2s^2A_1'(0,1)$ state. These peaks appear due to the slow radiative decay of metastable $2p^2A_2''$ molecules. Also, the probability of dissociating into three particles, rather than into $H + H_2$, is much higher for $2s^2A_1'$ than for $2p^2A_2''$. This is the reason that contributions from the $2p^2A_2''$ state are practically absent in the field-free spectrum. As a consequence the effective field-induced three-body signal from the $2p$ states emerges with a contrast much higher than predicted from Eq. (5). On the basis of the

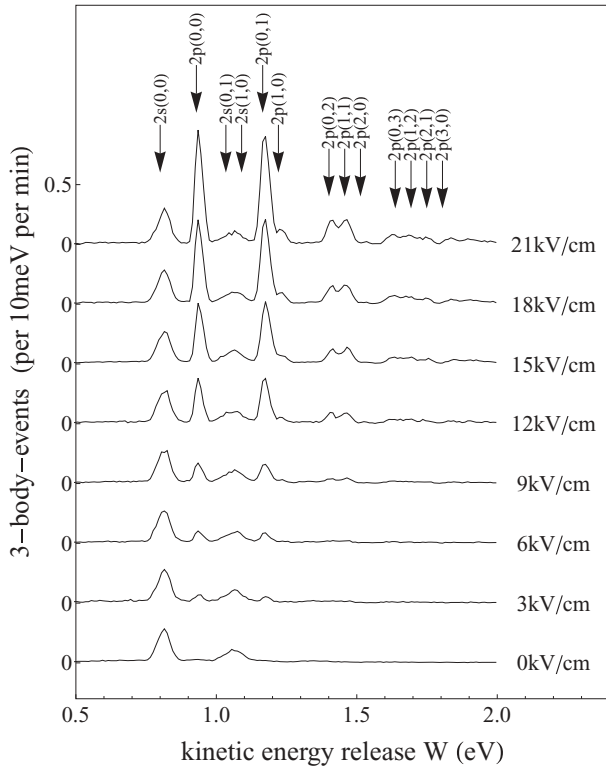
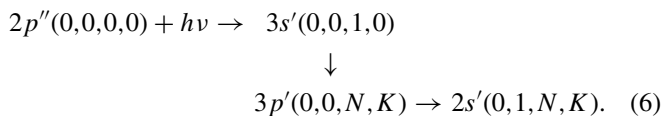


FIG. 3. Kinetic energy release spectra for the three particle decay of D_3 . The eight traces are measured at different maximal field strengths. They are normalized to measurement time and show the event rate per minute. The appearing peaks are labeled corresponding to $n\ell(v_1, v_2)$.

measured energy release, the appearance of the field-induced peaks can uniquely be attributed to predissociating molecules in various vibrational levels of the $2p^2A_2''$ state.

B. Population of $2s$ states by radiative cascade

A rather different method relies on the preparation of molecules in the $2s^2A_1'$ state in radiative cascade, following laser excitation of H_3 and D_3 molecules from metastable $2pA_2''$ levels to the electronic states $3sA_1'$, $3dE''$, or $3dA_1'$. A significant fraction of these states radiates in a cascade via the $3pE'$ state into $2sA_1'$ vibrational levels [6] which subsequently dissociate, an example being



We find that these cascade processes [13] are substantially stronger in D_3 than in H_3 , one reason being the slower rates of predissociation in the $n = 3$ states of D_3 [14]. An example for a 3-body fragment energy spectrum resulting from laser excitation to the $3sA_1'$ state [6] is given in Fig. 4. The peaks appearing below 2 eV correspond to different vibrational levels of $2sA_1'$ states [15]. The identification of the final vibrational state in the cascade is unique as the total energy release is measured with vibrational resolution. This measure is used as

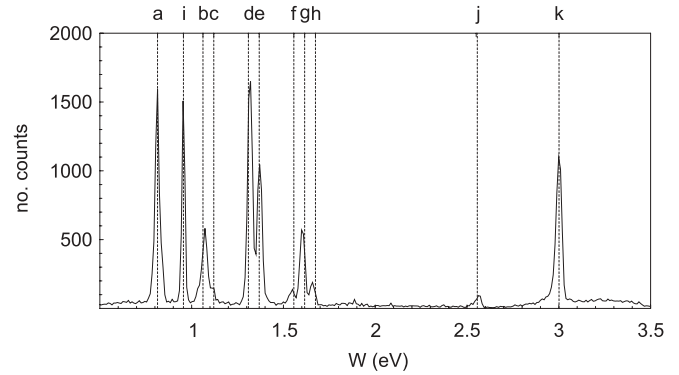


FIG. 4. Spectrum of total kinetic energy release in $D(1s) + D(1s) + D(1s)$ following photoexcitation to the $3sA_1'(0,0,1,0)$ state of D_3 [6]. Dotted lines give the expected energy release for different final state levels. The labels a-j refer to final states populated in cascading transitions; k is the photoexcited state. a: $2sA_1'(0,0)$. b: $2sA_1'(0,1)$. c: $2sA_1'(1,0)$. d: $2sA_1'(2,0)$. e: $2sA_1'(1,1)$. f: $2sA_1'(0,3)$. g: $2sA_1'(1,2)$. h: $2sA_1'(2,1)$. i: $2pA_2''(0,0,2,0)$. k: $3sA_1'(0,0,1,0)$. j: $3pE'(0,0,2/1,1)$. When N and K cannot be given with certainty the notation is $n\ell S(v_1, v_2)$.

a selection criterion for individual molecules when generating Dalitz maps for the corresponding states.

III. EXPERIMENTAL VECTOR CORRELATION MAPS

It was recognized [16] early on — in the case of decay of a τ meson into three π mesons, a situation formally analogous to the three-particle decay of a triatomic molecule — that the high dimensionality of this problem can be reduced by mapping the (center of mass) configuration space in terms of three spherical parameters, ρ , ϑ , and φ . The configuration space can be for both momentum and spatial arrangement [2]. While the hyperradius ρ controls the overall size of the configuration triangle, ϑ and φ describe its shape; see Fig. 5. In case of the final momentum configurations in three-body dissociations (i.e., interaction among the atoms has ceased), the configuration is allocated in a Dalitz map, which is the projection of a sphere of constant ρ into the equatorial

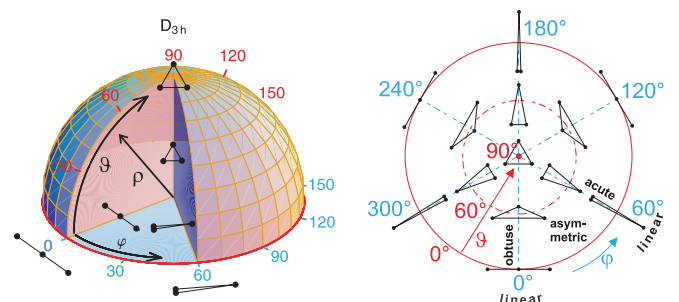


FIG. 5. (Color online) On the connection between hyperspherical coordinates and corresponding spatial configurations. The spatial configuration sphere spanned by the three hyperspherical parameters ϑ , φ , and ρ is shown at the left. If ρ is fixed and the sphere surface is projected into the equatorial plane, the Dalitz plot appears, which describes the momentum configurations of the fragments in 3-body decay. One obtains the momentum vectors by drawing arrows from the center of mass of any given triangle to its corners; see Fig. 1 of [2].

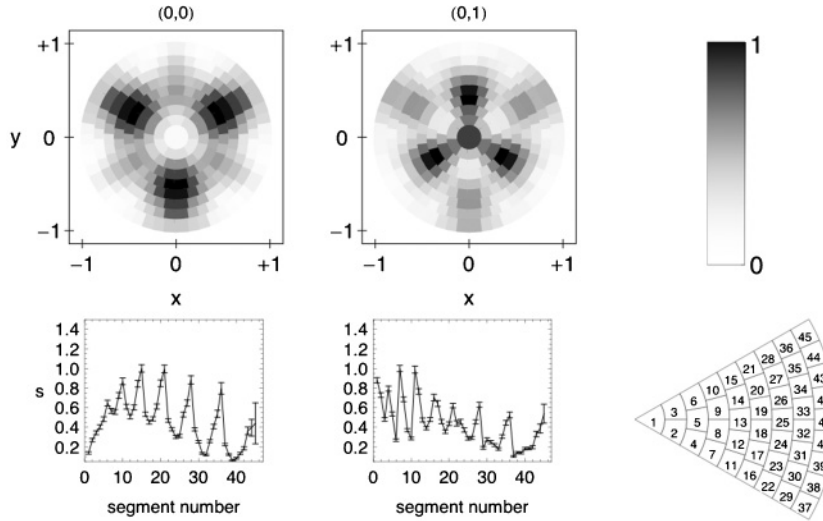


FIG. 6. Signal and error bars for the segments in two representative Dalitz maps are shown in the lower row, together with the absolute location of the numbered segment in each 60° slice of the phase space. The signal s gives the relative intensity normalized to the maximal count rate in each Dalitz plot, the total counts in each spectrum being $\approx 1 \times 10^4$.

plane [2,6,16]. Hyperspherical coordinates can be used for representation of dissociative potential energy surfaces [17], as well as for the calculation of rovibrational levels in a potential well [18]. For C_{2v} symmetry the angle φ has values $\varphi = n \times 60^\circ$ (n integer) and the hyperangle ϑ characterizes various isosceles triangles; it varies from 0° (obtuse linear) to 180° (acute linear) with 90° for the equilateral triangle. These coordinates are explained in detail in the appendices of [2] and [6].

The triple-coincidence data from each molecule which contributes to a peak in Figs. 3 and 4 also delivers a data point to the Dalitz map for the respective individual vibronic state. For the Cartesian coordinates of the Dalitz map we choose the labels [19]

$$x = 3(\varepsilon_2 - \varepsilon_1)/\sqrt{3} \quad \text{and} \quad y = 3(\varepsilon_3 - 1/3).$$

They relate the reduced kinetic energy of the i th atom in the center of mass frame, $\varepsilon_i = m\bar{u}_i^2/(2W)$, to the orientation of the three momentum vectors. The quantities ε_i are normalized to the total kinetic energy release W ,

$$W = \frac{m}{2} \sum_i \bar{u}_i^2 = \frac{1}{2m} \sum_i \bar{k}_i^2. \quad (7)$$

In contrast to previous publications we adopt a coarser-binned representation of Dalitz data, tailored to the symmetry of the problem and laid out to quantify the statistical error in each segment of the phase space of the Dalitz map. Two examples of Dalitz maps are given in Fig. 6. They describe electric-field-perturbed vibrational states of D_3 $2p^2A_2''$. The relative error in each segment remains below 10% with exception of segments 44 and 45, for which our coincidence detector geometry has very low efficiency.

This segmented presentation permits consideration of statistical and absolute measurement uncertainties. Altogether ten observables [20] are used to calculate the position of a three-body event inside the Dalitz map. Their absolute errors limit the resolution in the Dalitz phase space; however at the segment size used in Fig. 6 these are much smaller than the resolution dictated by statistical error. Throughout this paper we use the form of circular segment fractions with areas chosen

such that the statistical error of events represented by each segment remains generally less than 10%; see Fig. 6.

A. Comparison of photoexcitation and Stark-mixing method

Figures 7 and 8 compare Dalitz plots for the identical $2s^2A_1'$ vibrational states obtained by the two experimental methods.

The results are closely similar, albeit not identical. One reason for the small differences may be the contribution of several rotational states in the case in which the state is prepared via cascading [21]. A second effect may be the slight difference in energy between the pure $2s$ state and the $2p$ state with $2s$ character (≈ 100 meV, about 10% of the total energy release which appears in kinetic energy). A third effect is background events from false coincidences. While we have several coincidence and filter rules which sort out such events in hardware and software, a typical relative background signal of $\approx 5\%$ of the overall event rate remains. At first sight this might seem a minor contribution of uncertainty; however, one has to consider that these background events are themselves dependent on the method of state preparation. This is because they arise to a significant part from two-body dissociation, and the branching into two-body and three-body channels is different for different rovibronic states. As the detection efficiency for two-body events also depends on geometry, a differing background Dalitz pattern is expected for each rovibronic state.

As mentioned above, H_3 shows generally higher predissociation probability when compared to D_3 , making cascading processes less probable. This is why in H_3 only the $2s(0,0)$ and $(0,1)$ Dalitz maps were obtained via the cascading method [6]. The Stark mixing method offers a way to circumvent this difficulty. Examples of vector correlation maps not previously obtained for H_3 are shown in Fig. 9.

IV. DISCUSSION

To discuss the nature and the origin of the momentum correlations observed here we introduce the pertinent potential energy surfaces in Fig. 10. The two lowest, 1^2A_1 and 1^2B_2 in C_{2v} symmetry, constitute a pair of two sheets of the ground state which intersect in D_{3h} symmetry (i.e., adiabatic

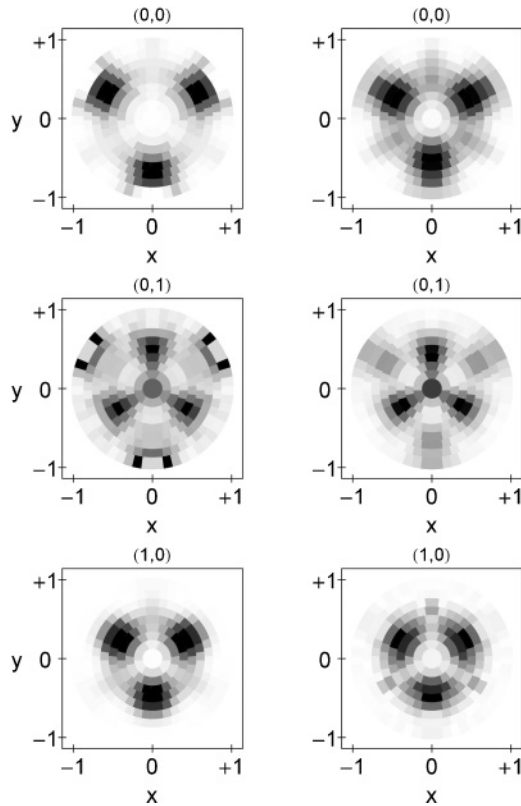


FIG. 7. Comparison of experimental Dalitz maps for $2s$ states of D_3 obtained via cascading (left column) and via the Stark mixing method (right column). The dissociation rate of $2p$ states at high field is dominated by the $2s$ -state amplitude. As a result close similarities appear in the dissociation-configuration pattern with the maps recorded after cascading transitions into the respective $2s$ states. The gray-scale function used can be seen on the upper right side of Fig. 6.

transitions between the sheets are possible above -1.57 a.u.). Both surfaces are repulsive and lead either to the fragments $H_2 + H$ at -1.674 a.u. or to three hydrogen atoms, $H(1s)$, at -1.5 a.u. All dissociation processes at energies below -1.29 a.u. move on one or both of these two surfaces.

The third and fourth surfaces, $1^2A'$ and $1^2A''$, see Fig. 10(b) at $\vartheta = 90^\circ$, are the first two which have an absolute minimum for the undissociated molecule. These are the states which we have abbreviated with $2s$ and $2p$, respectively.

Near their minimum the two surfaces are very close to each other (≈ 100 meV) and well isolated. At energies below -1.4 a.u. no adiabatic transition to other surfaces is possible from these surfaces; only nonadiabatic effects can dissociate the bound Rydberg molecules.

The nonadiabatic coupling between the $2pA_2''$ state and the dissociative ground state is mediated by rotational coupling. This coupling is absent for the metastable molecules, which are characterized by zero total angular momentum, $N = 0$ (excluding spin).

The nonadiabatic coupling between the $2sA_1'$ -state and the dissociative ground-state surfaces is mediated by the degenerate vibrational mode ν_2 . The circled areas in Figs. 10(a) and 10(c) indicate that motion along the size coordinate ρ and the distortion angle ϑ couples the bound 2^2A_1 state

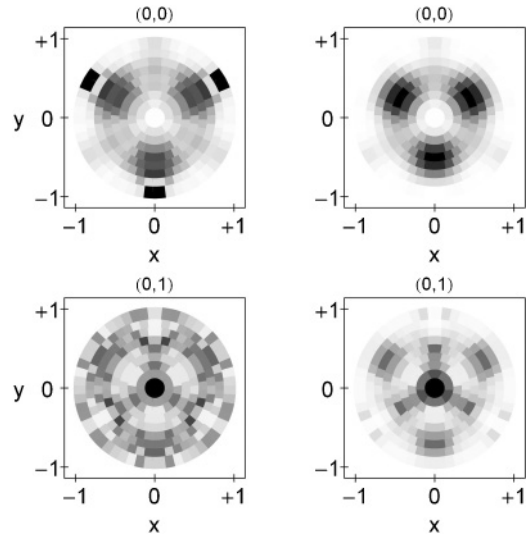


FIG. 8. Comparison of Dalitz plots for H_3 obtained by cascading into $2s$ (left column) with those formed by Stark-mixing (right column). At 20 kV/cm the Dalitz plots of the $2p$ states very much resemble those of the corresponding $2s$ states. The coarse binning into circular segments in Figs. 7 and 8 is chosen to control the statistical error in each bin to a value of less than 10%.

(corresponds to $2s^2A_1'$ in D_{3h} symmetry) with the ground-state surfaces at obtuse angles ($\vartheta < 90^\circ$) and acute angles ($\vartheta > 90^\circ$), respectively.

A. Comparison of experiment and theory

Early work on three-particle dissociation concentrated on the nature of nodal planes in Dalitz maps [22]. Recently two publications predicted entire Dalitz maps for the three-body decay of triatomic hydrogen [1,2] for the $2sA_1'$ electronic initial state. Both approaches are semiclassical, combining the quantum description of the bound $2s$ state and its nonadiabatic

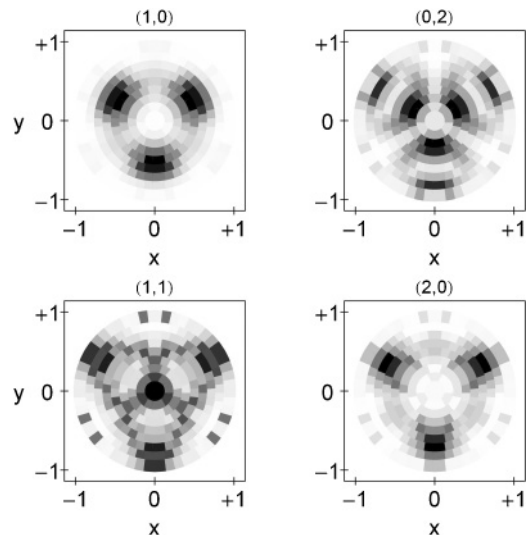


FIG. 9. Dalitz maps of $2s$ vibrational states of H_3 , obtained by Stark-admixing $2s$ character to the metastable $2p$ vibrational states present in our fast neutral beam.

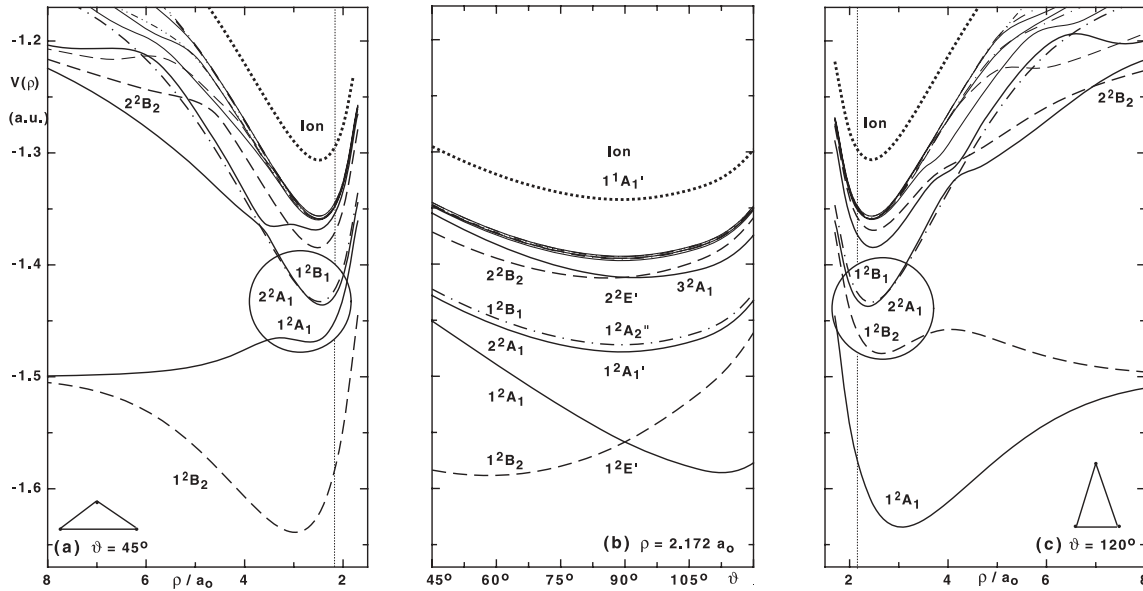


FIG. 10. Cuts through the potential surfaces of H_3 . The center panel shows the effect of a distortion conserving ρ and the C_{2v} symmetry. The panels on the right and left give the energies of the distorted molecule as a function of ρ . The vertical lines indicate coordinates common to the center panel (from [5]).

transition operator with classical trajectories on the two Jahn-Teller-split ground-state surfaces.

In Figs. 11 and 12 we compare the experimental Dalitz maps for different vibrational states with the predictions of Lehner and Jungen [1]. The center and right columns in both figures show their Dalitz maps for molecules which initially enter the upper and the lower ground-state surface, respectively. The experimental maps (left columns) indicate a dominance of obtuse-angle configurations in the vibrational ground state (see Fig. 11) for both H_3 and D_3 . On the other hand, when vibrational excitation of the bending mode is present, very substantial intensity appears at acute angles; see Fig. 12.

From a first glance of this comparison we could conclude that the experimental maps for the $2s(0,0)$ states in both

H_3 and D_3 indicate a preference for the molecule to begin predissociation preferentially on the upper surface. On the other hand, the maps for the $2s(0,1)$ states in H_3 and D_3 appear to indicate a preference to begin predissociation on the lower surface. However, we may also attempt to reconcile the experimental findings on the basis of the potential energy surfaces and vibrational-state symmetries.

B. Symmetry arguments relevant in the interpretation of the experimental Dalitz plots

The vector correlation structures in the Dalitz plots observed for the $2s$ states feature characteristic patterns which are recognized as distinct maxima at obtuse-angled and acute-angled geometries. These *coarse structures* are obviously

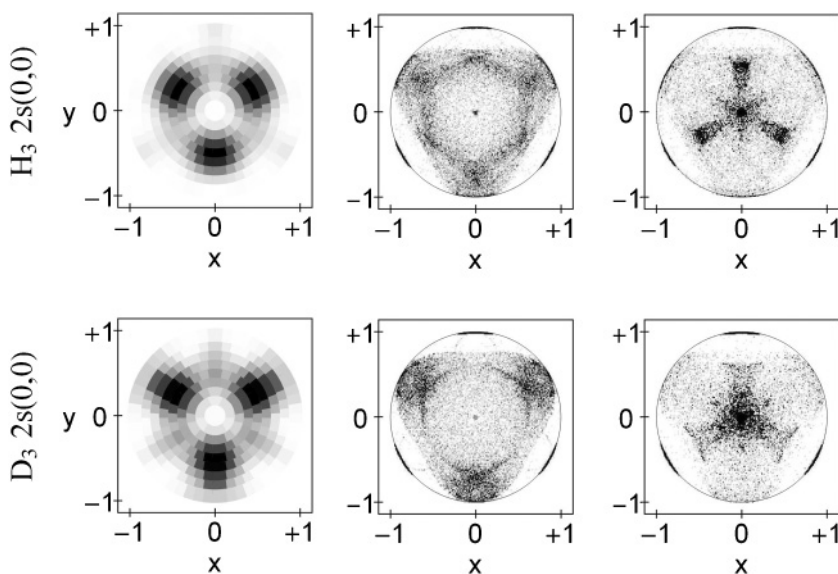


FIG. 11. Comparison of experimental Dalitz maps for the $2s(0,0)$ states of H_3 and D_3 (left column) with the semiclassical results predicted for dissociating molecules initially entering the upper surface (center) and the lower surface (right) [1]. The experimental maps (left columns) show a dominance of obtuse-angle configurations.

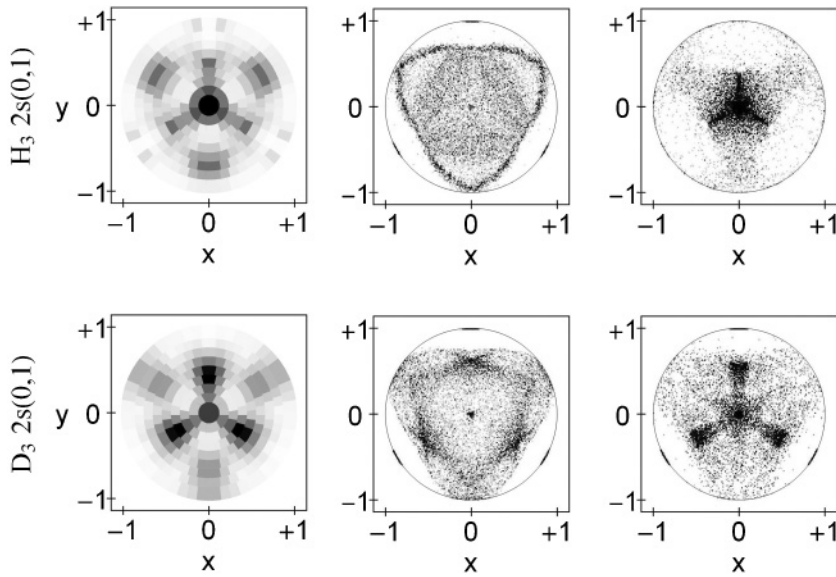


FIG. 12. Comparison of experimental Dalitz maps for the $2s(0,1)$ states of H_3 and D_3 (left column) with the semiclassical results predicted for dissociating molecules initially entering the upper surface (center) and the lower surface (right) [1]. The experiment shows a substantial contribution from acute-angle and equilateral-angle contributions.

independent of the way the $2s$ state is prepared, whether by cascading or Stark admixing. In the following, we discuss correlations between the coarse structures and symmetry properties of the initial vibrational wave function as well as the symmetry of nonadiabatic coupling, which is mediated by the degenerate vibrational mode v_2 .

In the harmonic approximation, the vibrational wave functions are given by a product of a one-dimensional harmonic oscillator (the symmetric stretch mode coordinate Q_1) and a two-dimensional harmonic oscillator describing the symmetric and asymmetric bending mode in polar coordinates (Q_r, φ) ; see appendix of [2] for further details. This leads to the wave function

$$\chi^{v_1, v_2, l_2}(Q_1, Q_r, \varphi) = \zeta^{v_1}(Q_1) \eta^{v_2, l_2}(Q_r, \varphi), \quad (8)$$

where l_2 denotes the vibrational angular momentum quantum number. The symmetric stretch coordinate Q_1 is totally symmetric. Considering symmetry properties one sees that predissociation of the $2s$ state can only be induced by the bending-mode motion [11]. As a consequence the function ζ^{v_1} has only minor influence on the part of the dissociation dynamics which is responsible for the nonequilateral configurations seen in the Dalitz plots. Hence it is appropriate to take a closer look at the function $\eta^{v_2, l_2}(Q_r, \varphi)$.

In the following discussion we make use of the equivalence of spatial vibrational coordinates and the momentum coordinates in the Dalitz plot; see Fig. 5. The recurring similarities of the coarse structures of states with $v_2 = 0$ as well as $v_2 = 1$ are apparent from Figs. 7, 8, and 9. The strong influence of symmetry properties of the vibrational wave function and the nonadiabatic coupling to the upper ground-state sheet has been pointed out by Lepetit *et al.* [23], and the predictions by Lehner and Jungen [1], as well as Galster [2], demonstrate that these geometric features are reflected in similar patterns in the final momentum correlations. Accordingly, the structure observed for $v_2 = 0$ states is an image of the ground-state vibrational wave function (a simple Gaussian in the coordinate Q_r), modified by the nonadiabatic coupling. Due to its symmetry property, the coupling active along the bending coordinates imposes node lines at acute-angled geometries,

thus splitting the ground-state vibrational wave function into three equivalent parts. The dissociating wave packet retains this signature of projection into the ground-state surface and mirrors it in the resulting Dalitz plot structure in three maxima at obtuse-angled geometries; see Fig. 11.

For states with $v_2 = 1$, the three maxima at obtuse-angled geometry are again recognized in the final momentum correlations. But now the function η in (8) is no longer independent of φ . This gives rise to an additional contribution from a coupling term which includes derivatives in φ [2]. In the final correlations, this effect is recognized as *three additional maxima* at acute-angled geometries, as well as a maximum at the center of the Dalitz plot, at the equilateral geometry; see Figs. 9 and 12.

For states with $v_2 = 2$, the vibrational angular momentum can take three values, $l_2 = \{-2, 0, 2\}$. In the harmonic approximation, the corresponding states are degenerate. Rovibronic couplings and the anharmonicity of the potential introduce small-energy splittings between these levels, the splitting being below the energy resolution of our experiment. While the functions $\eta^{2, -2} = (\eta^{2, 2})^*$ depend on φ , the function $\eta^{2, 0}$ is independent of φ . In the latter case, the vibrational wave function and nonadiabatic couplings feature the same φ dependence as for $v_2 = 0$ and thus similar structures with respect to the azimuth are expected in the Dalitz plot, and indeed observed; see Fig. 9.

Considering this, we can safely assume that the $(v_1 = 0, v_2 = 2)$ plot shown in Fig. 9 is obtained from an $l_2 = 0$ level. It is quite remarkable that now six maxima appear at obtuse-angled geometries: They indicate that the three maxima for $v_2 = 0$ states have been split by a node. This is not surprising, as the function $\eta^{2, 0}$ shows a node with respect to Q_r as well.

Most astounding is the fact that the experimental Dalitz plots mirror the spatial symmetries of the product of vibrational wave functions and spatial dependence of the nonadiabatic coupling operator in such direct fashion. Further support for this far-reaching statement is found from Figs. 11 and 12: We see that for identical vibrational levels, H_3 and D_3 show similar coarse structures in the Dalitz plot, despite the fact that their

predissociation lifetimes in the $2s$ state differ substantially (factor 5). More momentum correlation maps for $2s$ ($v_2 = 2$) levels in D_3 , obtained via the photoexcitation method, have been published in Fig. 7 of [6], bottom line. The structure seen in the plot marked as (1,2) [b] clearly resembles the structure shown for the ($v_1 = 0, v_2 = 2$) state in this paper for H_3 , Fig. 9. By contrast, the states labeled as (0,2) [a] and (1,2) [a] in Fig. 7 of [6] show much more complex correlation patterns. This leads us to the conjecture that the latter two states involve the $l_2 = \pm 2$ levels of $v_2 = 2$. No prior spectroscopic evidence existed for such an assignment.

V. CONCLUSIONS

The action of nonadiabaticity in molecular dissociation occurs in the phase space of the degrees of freedom which link the motion in the molecular frame to the motional and internal degrees of the fragments. The case considered here is simplified because no internal excitation can appear in the three fragment atoms in three-body decay of low-lying Rydberg states of H_3 and D_3 . Thus a unique projection of molecular degrees of freedom into the phase space of Dalitz coordinates of the three separating atoms exists. Insight gained from calculations of the nonadiabatic coupling and the atomic evolution on the ground-state surface guided us to a first interpretation of experimental vector correlation maps. We conclude that the coarse structures in experimental Dalitz plots directly image the spatial symmetry of the product of

the vibrational wave function and spatial dependence of the nonadiabatic coupling operator.

This finding opens a bridge to more detailed studies of the intricate aperture function which characterizes nonadiabaticity. Clearly, the electronic state scrutinized here is among the most simple situations encountered in triatomic hydrogen. We know from previous studies [4–6] that the vector correlation maps show increasing complexity for the higher lying Rydberg states. Further development of semiclassical and quantum simulations of the dissociation process promises more guidance in this regard. The theoretical results published so far are just a first entrance toward a complete account of the dynamics involved. Lehner and Jungen [24] have started a fully quantum-mechanical wave packet description, including effects of molecular rotation. We are confident that further guidance by such an approach will eventually permit the reconstruction of the phase-space dependence of nonadiabaticity in a polyatomic molecule. As nonadiabaticity is at the heart of every change occurring in nature, this goal is a worthwhile one.

ACKNOWLEDGMENTS

This research was supported by the Deutsche Forschungsgemeinschaft under Grant No. HE 2525/5. We thank Dr. M. Lehner, Professor M. Jungen, and Professor J. S. Briggs for helpful discussions.

-
- [1] M. Lehner and M. Jungen, *J. Phys. B* **42**, 065101 (2009).
- [2] U. Galster, *Phys. Rev. A* **81**, 032517 (2010).
- [3] U. Müller, T. Eckert, M. Braun, and H. Helm, *Phys. Rev. Lett.* **83**, 2718 (1999).
- [4] C. M. Laperle, J. E. Mann, T. G. Clements, and R. E. Continetti, *Phys. Rev. Lett.* **93**, 153202 (2004).
- [5] U. Galster, U. Müller, and H. Helm, *Phys. Rev. Lett.* **92**, 073002 (2004).
- [6] U. Galster, F. Baumgartner, U. Müller, H. Helm, and M. Jungen, *Phys. Rev. A* **72**, 062506 (2005).
- [7] P. Fechner and H. Helm, *Phys. Rev. A* **82**, 052523 (2010).
- [8] F. Baumgartner and H. Helm, *Phys. Rev. Lett.* **104**, 103002 (2010).
- [9] G. Gellene and R. Porter, *J. Chem. Phys.* **79**, 5975 (1983).
- [10] C. Bordas, P. Cosby, and H. Helm, *J. Chem. Phys.* **93**, 6303 (1990).
- [11] I. Dabrowski and G. Herzberg, *Can. J. Phys.* **58**, 1238 (1980).
- [12] I. Petsalakis, G. Theodorakopoulos, and J. Wright, *J. Chem. Phys.* **89**, 6850 (1988).
- [13] H. Figger, W. Ketterle, and H. Walther, *Z. Phys. D* **13**, 129 (1989).
- [14] The difference of the $3p$ -state lifetimes in H_3 and D_3 is substantial. From [13] we know that $\tau_{3p}(H_3) = (17.5 \pm 2)$ ns and $\tau_{3p}(H_3) = (1.1^{+0.2}_{-1.0})$ ns, while the purely radiative lifetime is $\tau_{\text{rad}}(H_3) = 22$ ns [12].
- [15] Each spontaneous dipole transition allows a total angular momentum ambiguity of ± 1 for the rotational state, depending on overall symmetry of initial and final state.
- [16] R. H. Dalitz, *Philos. Mag. Ser.* **44**, 1068 (1953).
- [17] D. Truhlar and C. Horowitz, *J. Chem. Phys.* **68**, 2466 (1978).
- [18] R. Jaquet, W. Cencek, W. Kutzelnigg, and J. Rychlewski, *J. Chem. Phys.* **108**, 2837 (1998).
- [19] Our definition includes a factor of 3 to ease labeling of the figures.
- [20] These are six impact positions, two time differences, the neutral beam velocity vector, and the distance between dissociation and detector.
- [21] In the case of Stark mixing the rotational state is well defined. It is the rotational level of the ionic core which remains unaffected at the field strengths required for our experiment.
- [22] J. S. Briggs and M. Walter, *Phys. Rev. A* **74**, 062108 (2006).
- [23] B. Lepetit, R. Abrol, and A. Kuppermann, *Phys. Rev. A* **76**, 040702(R) (2007).
- [24] M. Lehner (private communication).